The effect of limited MR field of view in MR/PET attenuation correction

Gaspar Delso,[a] Axel Martinez-Möller, Ralph A. Bundschuh,
Stephan G. Nekolla, and Sibylle I. Ziegler
Nuklearmedizin, Klinikum Rechts der Isar, Technische Universität München, 81675 München, Germany

(Received 16 February 2010; revised 6 April 2010; accepted for publication 24 April 2010; published 20 May 2010)

Purpose: A critical question in the development of combined MR/PET scanners is whether MR can provide the tissue attenuation data required for PET reconstruction. Unfortunately, MR images are often unable to encompass the entire patient. The resulting truncation in the transverse plane leads to incomplete attenuation maps, causing artifacts in the reconstructed PET image. This article describes the experiments performed to quantify these artifacts. A method to compensate the missing data was evaluated to determine whether software correction is possible or whether additional transmission hardware has to be included in the scanner.
Methods: Three studies were made. First, simulated PET data were used to quantify the bias due to an incomplete attenuation map. A set of spherical lesions was simulated in the lungs and mediastinum of a patient. The data were reconstructed with complete and partial attenuation maps and the uptake differences were evaluated. Second, clinical data from PET/CT oncology patients were used. To reproduce the expected conditions in an MR/PET scanner, only patients scanned with the arms resting along the body were considered. These scans were then used to create maps of the reconstruction bias due to field of view (FOV) limitations. Lastly, a PET reconstruction with incomplete attenuation data was evaluated as a means to obtain attenuation information beyond the MR FOV. The patient outline was automatically segmented with a three-dimensional snake algorithm and used to fill the truncated data in the attenuation map.
Results: Average bias up to 15% and local biases up to 50% were estimated when PET data were reconstructed with incomplete attenuation information. Completing the attenuation map with data extracted from a PET prereconstruction globally reduced these biases to below 10%. This correction proved to be tolerant to inaccuracies in positioning and attenuation values. However, local artifacts up to 20% could still be found near the edges of the MR FOV.
Conclusions: MR FOV restrictions can indeed make the reconstructed PET data unacceptable for diagnostic purposes. Biases can be globally compensated by automatic preprocessing of the attenuation map. However, inaccuracies in the correction will result in small artifacts near the periphery of the image that could lead to false-positive findings. [DOI: 10.1118/1.3431576]

Key words: PET, MR, MR/PET, attenuation, field of view

I. INTRODUCTION

Presently, there is great interest in combining data from different imaging modalities. This can be achieved either after data acquisition by means of image registration methods or by using new devices that can acquire data from two modalities simultaneously.

Combined positron emission tomography (PET) and computed tomography (CT) scanners are currently fully integrated in clinical routine. Although there are many advantages of this dual modality technique, CT provides limited soft-tissue contrast and exposes the patients to ionizing radiation. An alternative to the anatomical information provided by CT is that from magnetic resonance (MR) imaging.[1] Unfortunately, the combination of clinical MR and PET scanners has been proven to be very challenging due to the detrimental effect that the scanners may have on each other's performance when operated simultaneously.

In the past years, progress has been made in identifying scintillator materials with adequate magnetic properties,[2] developing PET detectors which either use optical fibers to guide the scintillation light away from the MR magnetic fields[3–7] or use magnetic-field-insensitive photodetectors,[8–12] and designing shielded electronics to avoid electromagnetic interference.[13] To this day, several research groups have successfully developed MR/PET prototypes for small animal studies, and one medical equipment company has demonstrated a human-sized design for neurology.[14]

No such systems have yet been presented for clinical whole-body imaging. For this purpose, two architectures have been proposed: Sequential architecture,[15] where the PET and MR scanners are placed in a tandem, much like the existing PET/CT machines, and integrated architecture, where a PET detector ring is incorporated between the MR radiofrequency coils and the main coil. The latter is without doubt the most technically challenging approach, but it offers the possibility of acquiring PET and MR data simultaneously. This feature makes integrated MR/PET scanners a perfect candidate for imaging regions under complex physi-

ological motion such as the thorax and abdomen. Both Philips Medical Systems and Siemens Medical Solutions have ongoing projects for the development of a whole-body integrated MR/PET scanner.

At the moment, an unresolved issue is how the attenuation correction of the PET images is going to be addressed. The attenuation problem could be decomposed into hardware and patient attenuation, the second aspect only is of concern in the present work.

One of the strongest selling arguments when PET/CT machines were introduced was the possibility of deriving the gamma-ray attenuation map of the patient from a fast CT scan. It made unnecessary the explicit measurement of this map by means of external radiation sources, considerably reducing the total scan time. This meant an increase in workflow, improved comfort, and less artifacts due to patient motion during the transmission scan.

Several approaches are currently being investigated in order to extrapolate gamma-ray attenuation maps from fast MR sequences.[16–20] The results from these studies indicate that it is indeed possible to perform PET attenuation correction based on the information provided by the MR. From the system design point of view, this would be the ideal solution, avoiding the considerable challenges of incorporating in the scanner additional hardware to perform transmission measurements.

However, the necessary information to create the attenuation map may not be readily available as MR images often do not encompass the complete body breadth of the patient. This is due to transverse field of view (FOV) restrictions imposed by inhomogeneities of the static magnetic field and nonlinearities of the gradient fields. A similar problem was already present in PET/CT scanners, where the transverse FOV of CT is usually limited to 50 cm. This leads to truncation artifacts, for which several correction algorithms have been proposed.[21,22]

Unfortunately, the situation is not exactly the same in the case of MR/PET scanners. Not only the transverse FOV is going to be smaller, probably between 40 and 45 cm, but also the existing field of view completion techniques from transmission tomography (when truncated projection data are accessible) could not be used in MR. Indeed, these techniques rely on the projective nature of CT to recover partial information about regions outside the FOV. This is not possible in MR, where no information whatsoever is recorded in those regions. Correction methods will therefore have to extrapolate from contextual data, like contour models or anatomical atlases, or obtain the missing information from an external source, like the PET scan or additional hardware included specifically for this purpose.

Given the considerable technical challenges of including additional hardware in the MR/PET scanners currently under development, a detailed study of the problem is required prior to making any design decisions. The goal of the present work is twofold: First, to evaluate the effect of the truncation artifacts on the PET images when MR-based attenuation correction is used. Second, to assess the viability and robustness of software-based techniques we propose to recover the attenuation information outside the MR FOV.

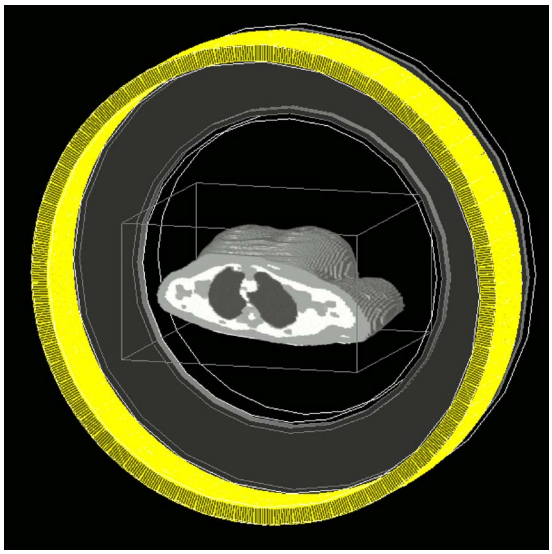

FIG. 1. (a) Setup of the simulations, including PET detector ring, shielding, and three-compartment model of the patient's attenuation extracted from the MR.

II. MATERIALS AND METHODS

II.A. Simulation studies

Monte Carlo simulation techniques combined with a realistic anatomy model offer an accurate and repetitive way to generate emission sinograms of synthetic lesions. These simulated data, of which the attenuation map is perfectly known, can then be used as a reference to evaluate the impact that omitting attenuation information has on the reconstructed images. The main problem of this methodology is the limited statistics, which, for practical reasons, restricts its use to the study of focal lesions.

The Monte Carlo simulation toolkit used for this study was the GEANT4 application for emission tomography (GATE).[23] The simulated scanner was a Siemens Ecat Exact HR+, a well-validated scanner model for which GATE simulations have been shown to agree with the measured data.[24] The HR+ detector consists of 4 block rings of 72 detector blocks each. The detector ring diameter is 82.4 cm. Each block is an array of 8×8 bismuth germanate crystals. The dimensions of each crystal are $4.05\times4.39\times30.0$ mm^3. The FOV is 15.2 cm axially and 60 cm transaxially.

The anatomical model used in the simulations was derived from a whole-body MR scan of a healthy volunteer. Both the scanned subject and the acquisition protocol were chosen so the body was entirely comprised of the FOV (shoulder breadth of 42 cm). The obtained data were then segmented into three tissue classes, as described in Ref. 19. This model was used to create both an indexed map of materials to be used during the simulation [Fig. 1(a)] and the corresponding attenuation map to be used in the reconstruc-

tion. The following materials were used as defined in the GATE database: Air (1.29 mg/cm^3), lung tissue (0.26 g/cm^3), adipose tissue (0.92 g/cm^3), and muscle tissue (1.05 g/cm^3). The linear attenuation values used to create the attenuation map were according to the mass attenuation coefficients provided by the National Institute of Standards and Technology: Air 1.12×10^{-4} cm^{-1} (approximated to 0 cm^{-1}), lung tissue 0.02 cm^{-1}, adipose tissue 0.089 cm^{-1}, and muscle tissue 0.10 cm^{-1}.

A set of 45 simulations was performed using this anatomical model. In each case, a single 5 kBq/ml spherical source of activity was simulated. Lesions of 10, 20, and 30 mm in diameter were simulated in the spine, mediastinum, lung parenchyma, lung hilum, and lung periphery. The anatomical model was scaled to represent shoulder span values of 42, 46, and 50 cm. As a reference, out of the ten adult patients discussed in Sec. II B, two had span values below 45 cm, six had span values between 45 and 50 cm, and the remaining two had span values greater than 50 cm. These values were measured as straight-line distances on the (projective) CT navigator images.

The coincidences provided by GATE ($>2\times10^5$ coincidences for 300 s of simulated acquisition with a 30 mm lesion) were converted to sinograms using the Ecat7 library. To reduce the size of the dataset, coincidences with ring difference greater than 22 rings were discarded, and the remaining data were axially compressed with a factor of 9. The resulting 3D sinograms were rebinned using single slice rebinning[25] and reconstructed with the open-source software for tomographic image reconstruction (STIR).[26] In particular, the *ordered subset maximum a posteriori one-step late* (OSMAPOSL) algorithm,[27–29] a variation in maximum likelihood estimation, was used. The algorithm was configured to use ten iterations, six subsets, and 1 mm inter-iteration Metz filtering. The same reconstructions were then performed again using a version of the attenuation map where the arms had been manually segmented and removed.

The uptake of the reconstructed lesions was obtained in each case by averaging all connected voxels with intensity values above 50% of the maximum. The reconstruction bias was expressed as $\varepsilon=100\times(I_2-I_1)/I_1$, the percentile variation in the reconstructed uptake (I_2) with respect to the uptake of the original reconstruction (I_1).

II.B. Patient studies

Since the introduction of PET/CT scanners, CT images have become the *de facto* standard for generating attenuation maps. Given a clinical PET/CT scan, the CT data can be edited to evaluate the impact of FOV limitations on the reconstructed PET images.

In order to reproduce the expected conditions in an MR/PET scanner, the patient has to be scanned with the arms resting along the body. This is common practice in MR due to space limitations and patient comfort considerations, but not in PET/CT, where priority is given to minimizing attenuation. However, it can happen occasionally due to medical needs, such as when the lesion of interest is located in the neck, that an oncology patient gets a whole-body scan with the arms resting along the body. For our study, we collected a set of ten fluorodeoxyglucose (FDG) PET/CT scans with arms down.

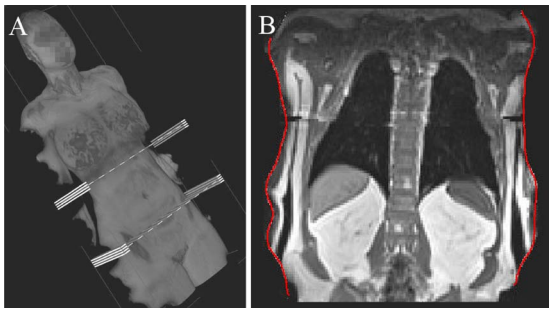

FIG. 2. (a) Volume rendering of a prototype MR sequence for attenuation correction. Note the missing parts due to field of view limitations. (b) Coronal slice displaying the contour of the MR field of view, segmented with a deformable surface model.

Whenever a new case arrived, the CT scan and PET raw data were exported and reconstructed with a research version of the reconstruction software present in the scanner (a Biograph 16 by Siemens AG, Erlangen, Germany). Different alterations of the CT scan from which the attenuation map is derived could thus be tested. The reconstruction algorithm from Fourier rebinned data was an attenuation-weighted OSEM with 2 iterations, 14 subsets, and 5 mm Gaussian postfiltering.

A first trial consisted of limiting the FOV to diameters ranging from 38 to 50 cm, which are expected values for a combined MR/PET system. As a reference, the Philips Achieva TX is advertised to have a transaxial FOV of 50 cm and the Siemens Magnetom Trio is advertised to have 40 cm of guaranteed static field homogeneity. Care was taken not to remove the patient bed, which is not affected by the MR FOV and which attenuation is assumed to be known exactly.

The reconstructed PET images were then compared to the original reconstruction. Bias maps were generated in each case, the normalized bias ($\varepsilon=100\times(I_2-I_1)/I_1$) being defined between the reference PET/CT reconstruction (I_1) and the reconstruction with missing attenuation information (I_2). To avoid unrealistic relative bias values, this measure was only applied to anatomical regions where the local intensity was above an empirically set threshold. The value of this threshold was usually set to reject the activity detected in the lungs and skin, keeping the liver and mediastinum. For visualization purposes, the measure was rewritten as $\varepsilon'=100\times|(I_2-I_1)/(I_1+k)|$, with k being an empirical dampening factor. Additionally, the average intensity value of a 7.3 ml region of interest manually placed in the liver was estimated in each case.

In practice, the sensitivity of the MR scanner is an ellipsoid, so the truncation may vary axially, as can be appreciated in Fig. 2. This effect can be reduced if the MR axial FOV matches the PET one. As combined whole-body MR/PET scanners are not yet available, equivalent FOV limitations had to be introduced in a PET/CT reconstruction to

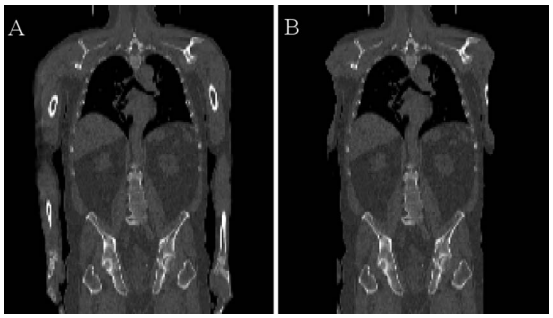

FIG. 3. Coronal views of a CT image used in the attenuation correction experiments. (a) Original image as provided by the PET/CT scanner. (b) Same image, limited to the field of view segmented from the MR image.

study the impact of a realistic MR FOV on PET attenuation correction. An opportunity presented itself in this sense when a PET/CT patient who had been scanned with both arms down to study a neck tumor agreed to undergo an MR scan in the same day. This provided two matching datasets, reflecting the exact same anatomy with practically no deformations, other than a minor shift in position due to the different bed shapes. Manual coregistration of the MR image with the CT confirmed that the match between both datasets was adequate for our purpose of applying the MR FOV to the CT.

A fast Dixon sequence such as those currently under study for MR-based attenuation correction[19] was acquired. The FOV of the resulting image was assumed to provide a good estimate of what can be measured in a combined scanner.

The limits of the effective FOV were obtained by segmenting the patient's profile. For this purpose, a deformable surface was used. The surface (S) is modeled as a coarse 4-connex mesh. The positions of the nodes of the mesh are iteratively modified to minimize the following energy functional:

$$E(S) = (1-\lambda)E_{\text{image}}(S|I) + \lambda E_{\text{internal}}(S),$$

where I is the image volume. E_{internal} is an energy term that depends on the current geometry of the surface. In our case, the internal energy includes first-order regularity and convexity constraints, as well as a term favoring the shrinking of the mesh. E_{image} is an energy term that depends on the image underlying the current surface position, here used to stop the shrinking. It is obtained by sampling the data volume at multiple positions defined by spline interpolation of the mesh nodes. The regularization parameter $\lambda \in [0,1]$ is used to balance the two energy terms. Figure 2(b) shows the segmented profile on a coronal view of the MR volume (notice how the MR FOV is not axially uniform).

The CT scan from the PET/CT was clipped with the obtained FOV [Figs. 3(a) and 3(b)]. The emission reconstruction using this CT scan for deriving an attenuation correction was then compared to the standard PET/CT reconstruction to reveal the magnitude and distribution of the bias caused by the missing attenuation information.

II.C. Field of view recovery

After discussing with an international group of medical experts, a maximum acceptable bias of 10% with respect to PET/CT has been set as an initial arbitrary reference for MR-based attenuation correction (note that the relative biases can only be applied in regions with sufficient uptake above the reconstruction noise). In consequence, the biases due to an incomplete attenuation map are generally unacceptable for clinical practice. Some means of recovering or compensating for the missing information is required.

This, however, is still an open problem with important implications on the design of a combined MR/PET system. Several hardware approaches have been discussed, namely:

- Including an external positron, single gamma, or x-ray source.
- Using either cameras or a laser scanner to detect the body contour.
- Incorporating mechanical elements to measure or constrain the patient's position.

However, we are not aware at this point of any group having tested one of these approaches. All of them have serious drawbacks due to either the technical challenges of their implementation or the restrictions that they would impose on the scan protocol. A software solution would, therefore, be desirable.

In brain PET scans, the attenuation map is sometimes approximated by geometrical- or atlas-based templates.[30] In order to evaluate the feasibility of this approach for whole-body imaging, a simple correction was tested on the simulated and patient datasets described in the previous sections.

In each case, a pair of elliptic cylinders was included in the attenuation map, manually registered to roughly the same size and position as the arms of the patient. Both cylinders were uniform and had the same linear attenuation coefficient as adipose tissue (a more conservative correction value than soft tissue or water and a better approximation for the average oncology patient). A reconstruction was then performed and the results evaluated with the bias estimation described in the respective sections.

The robustness of the correction with respect to the positioning of the cylinders was tested on one of the simulated datasets (2 cm lesion located at the lung center, FOV limited to 46 cm). For this purpose, eight additional reconstructions were performed after shifting the cylinders by ± 9 and ± 18 mm in both the x and y axes, respectively.

As will be appreciated in the results, this technique reduces considerably the overall reconstruction bias, but leads to local artifacts radiating from spots where the attenuation map has been incorrectly estimated. Indeed, blind correction techniques are potentially dangerous in whole-body imaging due to the increased anatomical variability. In consequence, it would be desirable to have some additional information that could be used to optimize the positioning of corrective structures in the attenuation map.

We propose to use the available PET data to complete the MR-based attenuation map. Indeed, the PET FOV is often

TABLE I. Relative bias of the reconstructed lesion intensity.

Lesion location	Lesion size (cm)	Uncorrected			Corrected		
		Span 42 cm (%)	Span 46 cm (%)	Span 50 cm (%)	Span 42 cm (%)	Span 46 cm (%)	Span 50 cm (%)
Lung hilum	3	−10.45	−10.83	−11.07	1.64	1.73	1.85
	2	−10.42	−10.84	−11.18	1.59	1.70	1.79
	1	−10.42	−10.84	−11.12	1.67	1.66	1.81
Lung center	3	−11.82	−12.33	−12.67	0.13	−0.10	−0.27
	2	−11.78	−12.19	−12.70	0.06	−0.18	−0.38
	1	−12.12	−12.34	−12.46	0.04	−0.18	−0.44
Lung periphery	3	−14.90	−15.92	−16.83	−0.03	−0.26	−0.32
	2	−14.82	−15.95	−16.88	−0.24	−0.35	−0.52
	1	−14.63	−15.93	−17.02	−0.23	−0.55	−0.65
Mediastinum	3	−14.95	−16.15	−17.35	1.22	1.26	1.12
	2	−15.11	−16.33	−17.49	1.17	1.14	0.98
	1	−15.83	−16.88	−18.22	0.83	0.88	0.78
Spine	3	−14.74	−15.95	−17.17	1.61	1.65	1.59
	2	−14.84	−16.10	−17.22	1.67	1.63	1.60
	1	−14.93	−16.20	−17.22	1.71	1.68	1.64

large enough to encompass the whole patient. As a reference, the Siemens Biograph TruePoint PET/CT is advertised to have a transaxial PET FOV of 605 mm.

Note that the proposed approach involves using information from the PET image to complete the attenuation map that is required to create this very image. Some sort of preliminary reconstruction is therefore required.

One option would be to use a reconstruction without attenuation correction for this purpose. An alternative solution is using a preliminary attenuation map based on the available MR information. Incorporating into this attenuation map a rough estimation of where the missing parts are expected to be further improves the accuracy of the preliminary reconstruction. In this experiment the estimated position of the arms extended 15 cm radially from the edge of the FOV and was limited vertically between the bed and the topmost chest position.

The body surface can be extracted from the intermediate reconstruction by means of simple image processing techniques. The resulting body mask can then be inserted in the attenuation map, assigning it a uniform attenuation coefficient (here 0.086 cm^{-1}). In our case, an automatic iterative segmentation based on active contours, similar to the one described in Sec. II B, was used. The use of a 4-connex spline mesh model enables a reduced number of control points to drive the mesh, relying on the intrinsic smoothness of the model to preserve the topology. A ring of ten control points was defined on each slice. The control point positions were initialized to encompass a bounding box of the patient, computed on sagittal and coronal projective views. The posterior evolution of the nodes was restricted to the transaxial plane. The node positions were iteratively updated to minimize a global energy functional. This functional included a transaxial shrinking term in the direction opposite of the model normals, which were updated after every iteration. A first-order regularization term was included to prevent the nodes from being stuck in reconstruction artifacts outside the patient. This term tended to move each node to the average position of its four immediate neighbors, projected on the current slice. Note how this term introduces a certain degree of smoothing in the axial direction. The external energy used to stop the shrinking was obtained for each control point by applying a soft threshold function to the average intensity of ten sample points obtained by spline interpolation.

Finally, a test was performed to determine the impact of segmentation inaccuracies in the reconstructed PET image. For this purpose, a 1 cm^3 cube of soft tissue was introduced in the CT image of a PET/CT scan. The cube was positioned adjacent to the thorax, over the patient's right arm (a position where regularized segmentation is likely to fail). The PET data were then reconstructed using the edited CT for attenuation correction, and the results are compared to the standard reconstruction.

III. RESULTS

III.A. Simulation studies

Table I shows the average intensity bias obtained with simulated lesions of 1–3 cm diameter, when completely removing the arms from a patient of 42–50 cm shoulder span. In the absence of any correction these biases range between 10% and 20%. As will be discussed in Sec. IV, this is not acceptable for clinical practice.

Introducing manually registered cylinders to simulate the attenuation of the missing arms reduces the bias below ±2%. This is the case even for deviations of up to 38% in the positioning of the phantom and a root mean square error of 0.04 cm^{-1} in the linear attenuation coefficient of the overlapping regions. The deviations were computed as $D=100\times(1-J)$, where $J=|A\cap B|/|A\cup B|$ is the Jaccard overlap index. A and B indicate binary masks of the phantom and the patient's arms. In the case of reconstructions where the phan-

TABLE II. Relative bias of the reconstructed liver intensity.

FOV diameter (cm)	Uncorrected			Corrected		
	Female 74 kg 165 cm	Male 86 kg 183 cm	Male 91 kg 184 cm	Female 74 kg 165 cm	Male 86 kg 183 cm	Male 91 kg 184 cm
38	18.7%	12.7%	15.9%	3.3%	0.8%	3.6%
40	15.1%	10.1%	13.2%	2.5%	0.3%	2.7%
42	11.6%	7.3%	10.4%	2.0%	0.08%	2.1%
44	8.1%	4.5%	7.6%	1.5%	0.3%	1.5%
46	5.2%	2.4%	4.8%	1.2%	0.3%	0.8%
48	2.9%	1.1%	2.3%	1.1%	0.1%	0.4%
50	0.9%	0.2%	0.7%	0.5%	0.03%	0.05%

tom was shifted along the x axis from its optimal position (2 cm lung lesion, span 46 cm), the bias increase was less than a 0.75% for 9 mm displacements and less than a 1.5% for 18 mm displacements.

III.B. Patient studies

Table II shows the average intensity biases obtained for a 7.3 ml sample of the liver as a function of the diameter of the attenuation map. The uptake level of the sample was always above that of the background noise. Three representative patients have been included. The results of the remaining patients are consistent with these values.

Pixelwise bias measurements show considerably higher local biases. For a patient of 45 cm shoulder breadth, limiting the FOV diameter to 45 cm results in normalized bias values up to 12% (truncation is still significant due to the patient usually not being vertically centered in the FOV). With this same patient, limiting the FOV diameter to 40 cm results in the normalized bias values up to 39%. These bias values were always measured for regions with uptake above an empirical threshold defined just below the average liver uptake.

Introducing manually registered cylinders to simulate the attenuation of the missing arms globally reduces the bias to below the 10% threshold, but the pixelwise bias images reveal severe local artifacts in the proximity of the arms. For example, for a 40 cm attenuation map, the bias due to uptake underestimation drops from 39% to a maximum of 8%, but small regions of up to 17% overestimation of the uptake appear.

Concerning the reconstructions using the FOV segmented from the MR scan (shoulder breadth 51 cm, FOV alternating between 40 and 45 cm), the bias in a 7.3 ml sample of the liver tissue is 4.7%, which can be reduced to 0.88% when correcting the attenuation map with manually registered cylinders, and to 0.64% when using the arms segmented from the PET.

The voxelwise bias images, however, give cause of concern. The relative error distribution depicted in Figs. 4(a) and 4(b) shows an expected maximum in the regions where attenuation information is missing and a progressive decrease as we move into the body. Leaving aside the arms, we find errors between 20% and 30% in the heart and spine, with peaks up to 50% being found locally in the ribs.

III.C. Field of view recovery

Concerning the recovery of missing attenuation information from the PET data, the use of a deformable contour model to extract the patient's profile from an uncorrected PET reconstruction has been proven feasible, but prone to errors due to the high level of background noise. Furthermore, without attenuation correction, the reconstructed emission image will be a convex hull, unable to allow delineation of the gap between the arms and the chest, as illustrated in Fig. 5(a). This leads to a segmentation that tends to overes-

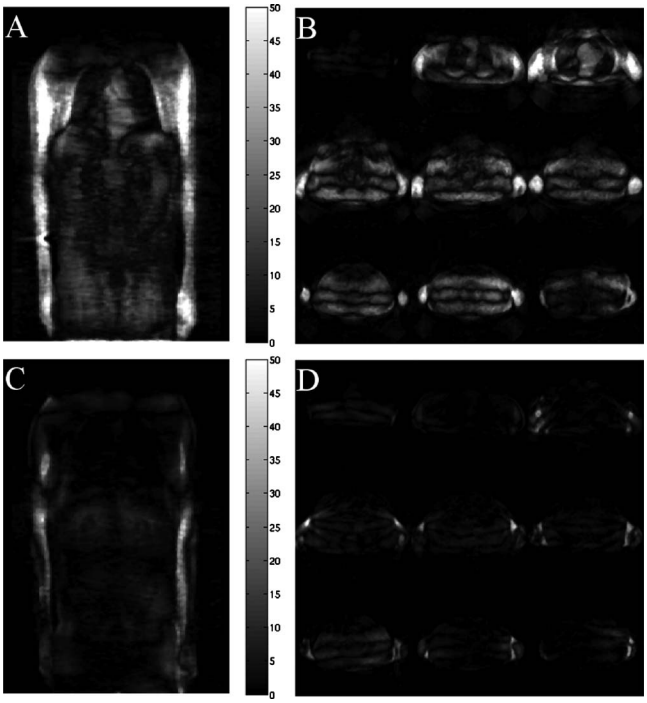

FIG. 4. Coronal and axial views of the reconstruction bias, expressed as a percentile deviation from the correct uptake. [(a) and (b)] Using an attenuation map with limited field of view. [(c) and (d)] Using the same attenuation map, completed with contour information obtained by automatic segmentation.

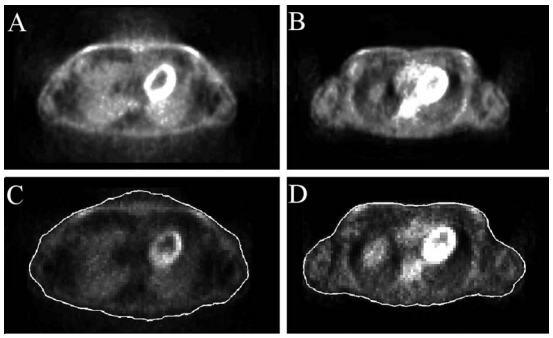

FIG. 5. Axial views of the preliminary PET reconstruction used to estimate the arms' position. (a) Reconstruction without attenuation correction. (b) Reconstruction with a modified attenuation map, in which soft-tissue attenuation was introduced in the region where the arms were expected to be. [(c) and (d)] Body contour obtained by automatic segmentation with active contours.

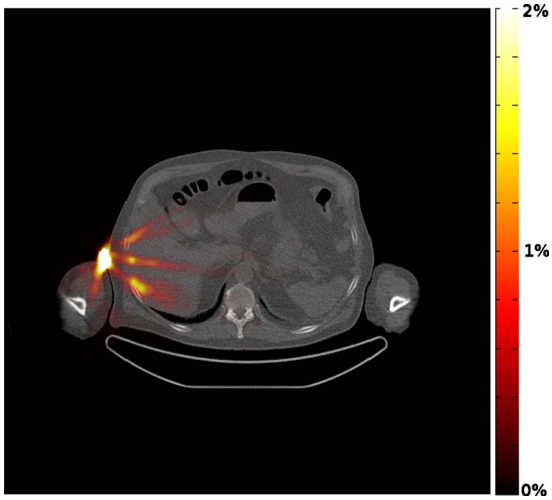

FIG. 6. Impact of a misplaced 1 cm^3 soft-tissue cube on the reconstruction: Reconstruction bias, expressed as a percentile deviation from the correct uptake, overlaid on an axial view of the CT image.

timate the size of the missing parts [Fig. 5(c)]. The impact of this error is minimal if the resulting profile is used only to guide the placement of a phantom model of the missing tissue. However, if the segmented body mask is used directly to complete the attenuation map, important artifacts can arise from the introduction of excess tissue.

As was mentioned in Sec. III B, this problem can be avoided by introducing in the reconstruction the available attenuation information, complemented with a rough estimation of the missing data. Some noise is still present in the estimated regions [Fig. 5(b)], but this poses no serious problem for the segmentation. The segmentation is more accurate and the decrease in background noise makes the results more robust to the active contour's parameterization [Fig. 5(d)]. Some biases may still be introduced due to the regularity constraints of the active contour.

The compensation of this missing information by means of segmentation-based phantom data reduces drastically this bias below the target 10% threshold [Figs. 4(c) and 4(d)]. As in the previous experiments, some streak patterns remain next to the corrected regions, with normalized bias values as high as 20%. These artifacts are located in the vicinity of regions where the correction has erroneously introduced attenuating material.

To give an impression of the magnitude of these artifacts, Fig. 6 shows the impact that the introduction of a 1 cm^3 cube of soft tissue has on the reconstructed image. Note how the artifacts are still important near the skin and could lead to false-positive diagnosis. The severity of the artifacts depends not only on the magnitude of the error in the attenuation map, but also on the number of lines of response intersecting it from each voxel.

IV. DISCUSSION

The need for this study arose during the design process of an integrated, whole-body MR/PET scanner. Due to MR technology limitations, it is often impossible to encompass the entire patient width in a single scan. This is a severe drawback if MR-based attenuation correction is to be used for PET reconstruction.

A first solution would be to avoid the presence of attenuating structures outside the MR FOV. For example, a common situation where this problem arises is when the patient is scanned with his arms resting along the body. Therefore, most PET/CT scans of the thorax are performed with arms up, to reduce the amount of attenuating tissue between the structures of interest and the PET detectors. However, the limited bore of MR scanners makes scanning with arms up quite uncomfortable for most patients. As a reference, the bore size of a Siemens Magnetom MR is 60 cm, compared to the 78 cm of a Siemens Biograph PET/CT. The presence of local radiofrequency coils limits patient mobility even further. Both head and (in most designs) neck coils would have to be removed to enable an arm-up scan. This would not be a problem for cardiac studies, but would probably be considered unacceptable in oncology. Furthermore, even if the arms could be positioned in a convenient way, the breasts, abdomen and hips still extend outside the FOV often enough to be a cause of concern. Another example would be breast imaging, where the patient is lying in prone position on a breast coil. In this case, the truncation of the patient's back could be severe and lead to significant artifacts.

As a consequence, if the presence of unknown attenuating structures outside the MR FOV cannot be avoided, either this attenuation has to be corrected during PET reconstruction or the resulting image artifacts have to be tolerated. PET/CT results have been adopted as a gold standard for this study.

Hence, from the results of our simulation experiments (Table I), we can deduce that the biases in the PET image due to attenuation outside the MR FOV are unacceptable. A correction method is mandatory for quantitative PET reconstruction.

Unfortunately, the techniques currently used in PET/CT for this purpose are not applicable in MR/PET. These tech-

niques are capable of recovering attenuation information for regions outside the FOV by exploiting the projective nature of CT acquisition. This is not possible in MR, and other sources must be explored to obtain the missing information.

The possibility of including a transmission system in the scanner was considered. However, this would require a considerable development effort. Furthermore, the impact of such a system on the performance of the MR scanner, due to the introduction of inhomogeneities in the static field, is a cause of concern. Before undertaking such an approach, the viability of addressing the problem by means of a software correction method had to be assessed.

In this sense, the results with the simulated data (Table I) show a considerable reduction in the bias of the average intensity when a simple geometrical phantom is used to represent the missing arms. Such reduction in the bias after a deliberately crude correction indicates that the compensation of missing attenuation information is relatively robust. It seems therefore feasible to implement an automated correction algorithm for its usage in clinical practice.

However, the study of the pixelwise bias on the reconstructed patient images leads us to be cautious. While the bias values themselves are coherent with the simulations' results, we note the presence of streaklike patterns in the PET images reconstructed with a completed attenuation map. These are caused by geometrical errors in the shape or positioning of the phantom (such as those caused by an excess of regularization over and under both arms) and by discrepancies between the phantom and the missing tissue's attenuation (such as those in the vicinity of the hands).

Even though these biases fan out from the position where the erroneous attenuation information was introduced and decrease rapidly as they penetrate the body, they can still reach important values near the borders of the MR FOV. Due to the local nature of the bias,[31] in clinical practice they could be perceived as pathological hot spots. Arguably, physicians could be educated to compare the PET image with the truncated MR image to avoid mistakes around truncated area. Still, this situation would probably be considered unacceptable for certain clinical applications.

The results presented here indicate that the correction of an incomplete attenuation map for PET reconstruction is indeed possible and globally robust to inaccuracies, but caution is needed when introducing correction factors in the proximity of regions of clinical interest. This confirms our initial hypothesis that blind correction methods (such as those solely based on geometrical models or anatomical atlas data) are not advisable in this case. The question remains whether sufficient patient information can be recovered without additional transmission hardware.

The experiments using a deformable contour model to extract the patient profile from a preliminary reconstruction of the PET data show promising results. As expected, using an uncorrected PET reconstruction for this purpose leads to noisy images, very sensitive to the parameters of the segmentation. Furthermore, the concavities in the body contour tend to be filled, leading to severe reconstruction biases. This problem is solved by using the available attenuation information completed with an estimation of the missing structures. This leads to an improved intermediate reconstruction, as depicted in Fig. 5(b), from which the patient profile can be extracted with reasonable accuracy. A step further would be using the resulting body mask as a reference to obtain the missing information from an anatomical atlas and register it into the attenuation map.

This approach would be limited to radiotracers with sufficient background uptake to perform the segmentation of the body contour. This is, among others, the case of FDG, arguably the most widespread PET tracer in clinical practice. In the case of tracers with insufficient background uptake, software correction would still be possible through techniques such as the estimation of attenuation information from emission data, e.g., by applying a consistency condition to the reconstruction problem.[32,33]

Despite the promising results obtained with the proposed method, several issues need to be addressed before it can be considered for clinical practice. Measures must be taken to avoid correction errors near the patient, as they cause strong local artifacts in the images that could lead to false-positive findings. Some such errors may be caused by regularity or shape constraints imposed on the segmentation. These constraints are necessary to ensure a proper convergence and prevent the segmentation from being affected by noise in the images. However, the anatomy of the patient never fits perfectly to these idealized models. In this case, a relaxation of the constraints once the segmentation has converged would allow the algorithm to further improve the segmentation results. Also, mechanically ensuring a minimal separation between the patient's arms and torso would considerably reduce the severity of local artifacts due to segmentation errors. This would mean moving the arms further outside the MR FOV, possibly increasing the global reconstruction bias. However, global bias have a relatively low impact in clinical practice and a small increase can be accepted in order to prevent strong local artifacts.

Future work on this topic include the use of an iterative attenuation correction method to reduce local biases, the use of better anatomical models (including muscle and bone), exploiting the axial variability of the MR FOV and testing an iterative approach to refine the estimation of the preliminary attenuation map.

V. CONCLUSION

The exposed results show that the lack of patient attenuation information due to MR FOV restrictions can lead to unacceptable bias in the PET images obtained with MR/PET scanners.

However, the correction of this bias by means of relatively simple image processing, such as the introduction of phantom data in the attenuation map, has been shown to be robust enough to be considered for clinical applications. An example of such a correction method based on the automatic segmentation of a PET prereconstruction has been demonstrated. On the other hand, caution is still advised when

implementing such methods in order to avoid local but potentially misleading artifacts near the borders of the corrected FOV.

ACKNOWLEDGMENTS

The authors would like to thank Dr. Jasmine Schirmer for her assistance in the writing of this paper. This project was supported in part by a research grant from Siemens Medical Solutions.

[a]Author to whom correspondence should be addressed. Electronic mail: gaspar.delso@tum.de; Telephone: +49(0)8941406397; Fax: +49(0)8941404938.

[1]H. Zaidi, O. Mawlawi, and C. G. Orton, "Point/counterpoint. Simultaneous PET/MR will replace PET/CT as the molecular multimodality imaging platform of choice," Med. Phys. **34**, 1525–1528 (2007).
[2]S. Yamamoto, K. Kuroda, and M. Senda, "Scintillator selection for MR-compatible gamma detectors," IEEE Trans. Nucl. Sci. **50**, 1683–1685 (2003).
[3]N. L. Christensen, B. E. Hammer, B. G. Heil, and K. Fetterly, "Positron emission tomography within a magnetic field using photomultiplier tubes and lightguides," Phys. Med. Biol. **40**, 691–697 (1995).
[4]A. J. Lucas, R. C. Hawkes, R. E. Ansorge, G. B. Williams, R. E. Nutt, J. C. Clark, T. D. Fryer, and T. A. Carpenter, "Development of a combined microPET-MR system," Technol. Cancer Res. Treat. **5**, 337–341 (2006).
[5]P. K. Marsden, D. Strul, S. F. Keevil, S. C. R. Williams, and D. Cash, "Simultaneous PET and NMR," Br. J. Radiol. **75**, S53–S59 (2002).
[6]R. R. Raylman, S. Majewski, S. S. Velan, S. Lemieux, B. Kross, V. Popov, M. F. Smith, and A. G. Weisenberger, "Simultaneous acquisition of magnetic resonance spectroscopy (MRS) data and positron emission tomography (PET) images with a prototype MR-compatible, small animal PET imager," J. Magn. Reson. **186**, 305–310 (2007).
[7]Y. Shao, S. R. Cherry, K. Farahani, R. Slates, R. W. Silverman, K. Meadors, A. Bowery, S. Siegel, P. K. Marsden, and P. B. Garlick, "Development of a PET detector system compatible with MRI/NMR systems," IEEE Trans. Nucl. Sci. **44**, 1167–1171 (1997).
[8]B. Pichler, E. Lorenz, R. Mirzoyan, W. Pimpl, F. Roder, M. Schwaiger, and S. I. Ziegler, presented at the IEEE Nuclear Science Symposium Conference Record, 1997 (unpublished).
[9]C. Catana, Y. Wu, M. S. Judenhofer, J. Qi, B. J. Pichler, and S. R. Cherry, "Simultaneous acquisition of multislice PET and MR images: Initial results with a MR-compatible PET scanner," J. Nucl. Med. **47**, 1968–1976 (2006).
[10]R. Grazioso, N. Zhanga, J. Corbeila, M. Schmanda, R. Ladebeck, M. Vester, G. Schnur, W. Renz, and H. Fischer, "APD-based PET detector for simultaneous PET/MR imaging," Nucl. Instrum. Methods Phys. Res. A **569**, 301–305 (2006).
[11]B. J. Pichler, M. S. Judenhofer, C. Catana, J. H. Walton, M. Kneilling, R. E. Nutt, S. B. Siegel, C. D. Claussen, and S. R. Cherry, "Performance test of an LSO-APD detector in a 7-T MRI scanner for simultaneous PET/MRI," J. Nucl. Med. **47**, 639–647 (2006).
[12]C. Woody *et al.*, "Preliminary studies of a simultaneous PET/MRI scanner based on the RatCAP small animal tomograph," Nucl. Instrum. Methods Phys. Res. A **571**, 102–105 (2007).
[13]S. S. Junnarkar, J. Fried, P. O'Connor, V. Radeka, P. Vaska, M. Purschke, D. Tomasi, J.-F. Pratte, S.-J. Park, C. Woody, and R. Fontaine, presented at the IEEE Nuclear Science Symposium Conference Record, 2006 (unpublished).
[14]H.-P. W. Schlemmer, B. J. Pichler, M. Schmand, Z. Burbar, C. Michel, R. Ladebeck, K. Jattke, D. Townsend, C. Nahmias, P. K. Jacob, W.-D. Heiss, and C. D. Claussen, "Simultaneous MR/PET imaging of the human brain: Feasibility study," Radiology **248**, 1028–1035 (2008).
[15]Z. Hu *et al.*, "MR-based attenuation correction for a whole-body sequential PET/MR system," IEEE Nuclear Science Symposium Conference Record, Orlando, 2009, pp. 3508–3512 (unpublished).
[16]H. Zaidi, "Is MR-guided attenuation correction a viable option for dual-modality PET/MR imaging?," Radiology **244**, 639–642 (2007).
[17]T. Beyer, M. Weigert, H. Quick, U. Pietrzyk, F. Vogt, C. Palm, G. Antoch, S. Müller, and A. Bockisch, "MR-based attenuation correction for torso-PET/MR imaging: Pitfalls in mapping MR to CT data," Eur. J. Nucl. Med. Mol. Imaging **35**, 1142–1146 (2008).
[18]E. Rota-Kops, P. Qin, M. Müller-Veggian, and H. Herzog, presented at the Springer Proceedings in Physics: Advances in Medical Engineering, 2007 (unpublished).
[19]A. Martinez-Moller, M. Souvatzoglou, G. Delso, R. A. Bundschuh, C. Chefd'hotel, S. I. Ziegler, N. Navab, M. Schwaiger, and S. G. Nekolla, "Tissue classification as a potential approach for attenuation correction in whole-body PET/MRI: Evaluation with PET/CT data," J. Nucl. Med. **50**, 520–526 (2009).
[20]M. Hofmann, F. Steinke, V. Scheel, G. Charpiat, J. Farquhar, P. Aschoff, M. Brady, B. Scholkopf, and B. J. Pichler, "MRI-based attenuation correction for PET/MRI: A novel approach combining pattern recognition and atlas registration," J. Nucl. Med. **49**, 1875–1883 (2008).
[21]T. Beyer, A. Bockisch, H. Kühl, and M.-J. Martinez, "Whole-body 18F-FDG PET/CT in the presence of truncation artifacts," J. Nucl. Med. **47**, 91–99 (2006).
[22]O. Mawlawi, J. J. Erasmus, T. Pan, D. D. Cody, R. Campbell, A. H. Lonn, S. Kohlmyer, H. A. Macapinlac, and D. A. Podoloff, "Truncation artifact on PET/CT: Impact on measurements of activity concentration and assessment of a correction algorithm," AJR, Am. J. Roentgenol. **186**, 1458–1467 (2006).
[23]G. Santin, D. Strul, D. Lazaro, L. Simon, M. Krieguer, M. V. Martins, V. Breton, and C. Morel, "GATE: A Geant4-based simulation platform for PET and SPECT integrating movement and time management," IEEE Trans. Nucl. Sci. **50**, 1516–1521 (2003).
[24]S. Jan, C. Comtat, D. Strul, G. Santin, and R. Trebossen, "Monte Carlo simulation for the ECAT EXACT HR+ system using GATE," IEEE Trans. Nucl. Sci. **52**, 627–633 (2005).
[25]M. E. Daube-Witherspoon and G. Muehllehner, "Treatment of axial data in three-dimensional PET," J. Nucl. Med. **28**, 1717–1724 (1987).
[26]K. Thielemans, S. Mustafovic, and C. Tsoumpas, "STIR: Software for tomographic image reconstruction release 2," IEEE Nuclear Science Symposium Conference Record, 2006, Vol. 4, pp. 2174–2176 (unpublished).
[27]P. J. Green, "Bayesian reconstructions from emission tomography data using a modified EM algorithm," IEEE Trans. Med. Imaging **9**, 84–93 (1990).
[28]S. Alenius and U. Ruotsalainen, "Bayesian image reconstruction for emission tomography based on median root prior," Eur. J. Nucl. Med. Mol. Imaging **24**, 258–265 (1997).
[29]M. Jacobson, R. Levkovitz, A. Ben-Tal, K. Thielemans, T. Spinks, D. Belluzzo, E. Pagani, V. Bettinardi, M. Gilardi, A. Zverovich, and G. Mitra, "Enhanced 3D PET OSEM reconstruction using inter-update Metz filtering," Phys. Med. Biol. **45**(8), 2417–2439 (2000).
[30]H. Zaidi, M. L. Montandon, and S. Meikle, "Strategies for attenuation compensation in neurological PET studies," Neuroimage **34**, 518–541 (2007).
[31]K. Thielemans, E. A. Ravindra, M. Manjeshwar, A. Ganin, and T. J. Spinks, "Image-based correction for mismatched attenuation in PET images," IEEE Nuclear Science Symposium Conference Record, Dresden, 2008, pp. 5292–5296 (unpublished).
[32]A. Salomon, V. Schultz, R. Brinks, B. Schweizer, and A. Goedicke, "Iterative generation of attenuation maps in TOF-PET/MR using consistency conditions," Proceedings of SNM's 56th Annual Meeting, 2009 (unpublished).
[33]J. Nuyts, P. Dupont, S. Stroobants, R. Benninck, L. Mortelmans, and P. Suetens, "Simultaneous maximum a posteriori reconstruction of attenuation and activity distributions from emission sinograms," IEEE Trans. Med. Imaging **18**, 393–403 (1999).